Practical Methods of Interference Cancelation for Power Measurements in a Reverberation Tent

Yuanzhuo Liu, *Student Member, IEEE*, Sheng Guo, Ruijie He, *Student Member, IEEE*, Jiangshuai Li, *Student Member, IEEE*, and Victor Khilkevich, *Member, IEEE*

***Abstract*—In total radiated power (TRP) measurements, it is essential to eliminate the effects of electromagnetic interference caused by the ambient noise. The elimination is usually achieved by shielding. However, shielding may be insufficient, especially in reverberation tents. Under this condition, additional methods are needed to suppress the noise. Practical methods are proposed to suppress the effect of uncorrelated noise signals during the TRP measurement in the reverberation tents. The methods are validated for the cancelation of communication noise, including Wi-Fi, global system for mobile (GSM), and FM signals. If the noise reference signal is available, the noise contribution can be suppressed by ratio averaging. When the reference signal is hard to obtain, blind source separation allows separating the uncorrelated signals from the combination of the intended signal and noise. For intermittent signals, threshold cancelation is proposed.**

***Index Terms*—Blind source separation (BSS), electromagnetic interference (EMI), noise cancelation, total radiated power (TRP).**

I. Introduction

ELECTROMAGNETIC emissions have been receiving increasing attention due to rapid growth of the electronic industry. In complex electronic systems, noise is a product of multiple, often uncorrelated, emissions. It is of critical importance to accurately measure the emission noise [1], [2].

In total radiated power (TRP) measurement, it is essential to eliminate the effects of electromagnetic interference caused by unwanted noise contributions (i.e., ambient noise) [3]. The elimination is usually achieved by using shielded rooms [4]. Reverberation chambers, in general, are widely used as established environments to perform electromagnetic susceptibility and emission measurements, including TRP. A well-stirred reverberation chamber emulates a statistically uniform and isotropic field within its working volume [5]. However, due to the cost and complexity of construction of the reverberation chambers, reverberation tents are gaining popularity as an inexpensive substitution [6].

Manuscript received December 14, 2019; revised April 23, 2020; accepted May 30, 2020. Date of publication June 22, 2020; date of current version August 13, 2020. This paper was presented in part at the IEEE Symposium on Electromagnetic Compatibility, Signal and Power Integrity, New Orleans, LA, USA, July 2019. This work was supported in part by the National Science Foundation under Grant IIP-1916535. *(Corresponding author: Yuanzhuo Liu.)*

The authors are with the EMC Laboratory, Missouri University of Science and Technology, Rolla, MO 65401 USA (e-mail: liuyuanz@umsystem.edu; sgrzy@umsystem.edu; rhrg8@umsystem.edu; lijiangs@umsystem.edu; khilkevichv@umsystem.edu).

Color versions of one or more of the figures in this article are available online at https://ieeexplore.ieee.org.

Digital Object Identifier 10.1109/TEMC.2020.3000433

However, the shielding of the reverberation tents may be insufficient [6]. In this situation, additional methods are needed to suppress noise due to the sources located outside the tent.

Active noise control and adaptive noise cancelation are two conventional methods to deal with interference in a noisy environment [7]. The active noise control technology is widely used for acoustic noise suppression. In the active noise control systems, a detecting probe is used to pick up ambient noise. A noise-cancelation signal generator emits a wave with the same amplitude but with an inverted phase (also known as antiphase) to the noise signal, canceling it [8]. In electromagnetic compatibility (EMC) applications, however, this method, which needs an additional circuit to generate the canceling signal at gigahertz frequencies, is hard to implement.

Adaptive noise cancelation removes ambient noise by using a form of adaptive filter [9]. Two antennas measure signals simultaneously. One of the antennas captures the intended signal, which is corrupted by noise. The other antenna is located such that it receives a signal correlated with the noise component only. With the help of the Wiener filter, which is generated using statistical properties of the signal to minimize the sum of squares of the difference of the signals, the noise part can be subtracted from the mixed signal. However, the adaptive filter used in this method is trained over successive iterations with unpredictable convergence [10]. Quite often implementations of the adaptive filter require regularization [3] which relies on coefficients which need to be guessed for each particular situation.

In this article, alternative methods of noise cancelation involving only minimal signal processing that does not require iterative implementations or regularization are proposed. The diagrams representing two typical setups considered herein are presented in Fig. 1. In the setup (a), a dedicated noise reference is available (the setup is similar to a typical adaptive noise cancelation setup), while in the setup (b) both measurement channels are coupled to the intended and noise signals. The proposed cancelation procedure differs depending on the nature of the noise signal. For the intermittent signal, a threshold treatment allows excluding the noise contribution. For the continuous signals, averaging of the signal ratio [11] allows to cancel the noise contribution. For setup (b) when the reference noise signal is not available, the blind source separation [12], [13] is additionally used to obtain the clean references and finally cancel the unwanted contributions.

This article is an expanded version of the article presented earlier [14], which reported preliminary TRP measurement results.

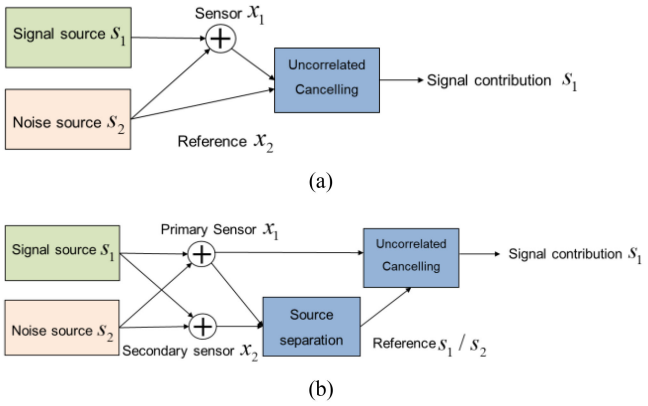

Fig. 1. Measurement setup diagrams. (a) Case with a dedicated noise reference. (b) Case with no dedicated noise reference.

In this article, the methods are expanded and applied to realistic noise signals. Successful suppression of the noise contribution of unwanted communication noise, including Wi-Fi, global system for mobile (GSM), and FM signals with and without direct noise reference is presented. As a result of cancelation, the dynamic range of the measurement is extended, improving the measurement sensitivity.

The rest of this article is organized as follows. Section II introduces the proposed methods, including the algorithm of averaging cancelation and the blind source separation. The validation of methods is demonstrated in Section III. In Section IV, the application of the methods to cancel the noise from practical sources is given. Finally, Section V concludes the article.

II. Methodology

A. Introduction to Blind Source Separation

A blind source separation (BSS)-based method is used in this article to separate the contributions of the noncorrelated signals measured in the reverberation tent when the dedicated noise reference is not available. The BSS methods were originally applied in the areas of neural networks, image enhancement, biomedical signal processing, and wireless telecommunication systems like sonar and radar [15].

In [13], the concept of BSS is proposed as a tool to identify individual signals in a mixture containing unknown, multiple, and overlapping signals. The BSS can be formulated as a generalized eigenvalue decomposition procedure under different assumptions about the source signals (for example, non-Gaussian, nonstationary independent sources, and so on).

The fields in the reverberation tent obey superposition due to the linearity of Maxwell's equations. For this reason, the signal model of the reverberation tent in the frequency domain can be formulated as a linear simultaneous mixture of signals, which agrees with the definition of the signal mixing under the BSS framework [13]. In the equations below, all quantities are frequency-dependent, but the argument $j\omega$ is omitted for brevity.

Suppose the observed signals represent a matrix $\mathbf{X}$, related to the source signals as

$$\mathbf{X} = \mathbf{AS} \tag{1}$$

where $\mathbf{S}$ is the matrix consisting of the original noncorrelated signals produced by the sources (including both intentional and unwanted ones), and $\mathbf{A}$ is an unknown mixing matrix of complex numbers. Matrices $\mathbf{X}$ and $\mathbf{S}$ are multidimensional matrices containing scalar signals x_i and s_i

$$\mathbf{X}(0\ldots\mathrm{T}) = \begin{pmatrix} x_1(0) & \cdots & x_1(\mathrm{T}) \\ \vdots & \ddots & \vdots \\ x_n(0) & \cdots & \mathrm{x}_n(\mathrm{T}) \end{pmatrix} \tag{2a}$$

$$\mathbf{S}(0\ldots\mathrm{T}) = \begin{pmatrix} s_1(0) & \cdots & s_1(\mathrm{T}) \\ \vdots & \ddots & \vdots \\ s_n(0) & \cdots & \mathrm{s}_n(\mathrm{T}) \end{pmatrix}. \tag{2b}$$

The columns of the matrices $\mathbf{X}$ and $\mathbf{S}$ represent samples of the signals at different time moments, n rows of the matrices correspond to n sources and probes (in general the number of sources and probes is not equal, but here we assume a fully determined case).

Out of these two matrices, the observation matrix $\mathbf{X}$ is directly measurable, but the source matrix $\mathbf{S}$ is not. However, if the inverse matrix of the mixing matrix $\mathbf{A}$ can be obtained, the sources $\mathbf{S}$ can, therefore, be recovered by inverting (1).

Recovery of the matrix $\mathbf{S}$ using the BSS can be implemented in two steps. The first one is to compute the unmixing matrix $\mathbf{W}$ with generalized eigenvalue procedure

$$\mathbf{W} = \mathrm{Eig}\left(\mathbf{X}\cdot\mathbf{X}^H, \mathbf{Q}\right) \tag{3}$$

where $\mathbf{Q}$ is diagonal cross statistics that differs depending on the assumptions about the nature of the signals, and H is the conjugate transpose operator.

Then the sources can be separated as follows [13]:

$$\hat{\mathbf{S}} = \mathbf{W}^H\mathbf{X}. \tag{4}$$

As a result of the separation, a matrix $\hat{\mathbf{S}}$ is produced, which is a scaled and permuted version of $\mathbf{S}$.

The structure of the matrix $\mathbf{Q}$ depends on the nature of the signals $\mathbf{S}$. The authors in [13] list a number of assumptions for the signals, including: 1) Nonstationary and noncorrelated, 2) nonwhite and noncorrelated, 3) non-Gaussian and independent, and 4) noncorrelated and mixed with an orthogonal matrix. These four assumptions cover most of the signals (with the exception of the stationary white noise). Assumptions 1) and 2) are suitable for most communication signals. Since the signals in our study were both stationary (when a signal generator was used to create interference) and nonstationary (in the case of real communication signals), we selected the assumption 2) (nonwhite and noncorrelated signals) for which, according to [13] the matrix, $\mathbf{Q}$ is given as the symmetric cross correlation with time lag τ

$$\mathbf{Q} = \mathbf{X}(0\ldots T-\tau)\cdot\mathbf{X}^H(\tau+1\ldots T) + \mathbf{X}(\tau+1\ldots T) \cdot\mathbf{X}^H(1\ldots T-\tau) \tag{5}$$

where τ is the delay within the nonzero autocorrelation interval in the sources, and T is the observation time. Equation (5) is used henceforth to perform the signal separation.

Since the dimension of matrices $\mathbf{X} \cdot \mathbf{X}^H$ and $\mathbf{Q}$ is $n \times n$, and the number of sensors n cannot be very large (limited primarily by the number of the receiver channels), implementation of (3) can be very time efficient (milliseconds of CPU time for $n = 2$ in MATLAB implementation).

Since the separated signals in $\hat{\mathbf{S}}$ (and hence their powers) are scaled with unknown coefficients, they are unsuitable for the TRP contribution measurement. The next section describes how to remove the effect of unknown scaling.

B. TRP Contribution Estimation by Ratio Averaging

Let us consider a linear combination of two sources (the case can be easily generalized to an arbitrary number of sources) in the frequency domain

$$x_1 = k_{11}s_1 + k_{12}s_2 \tag{6}$$

$$x_2 = k_{21}s_1 + k_{22}s_2 \tag{7}$$

where s_1 and s_2 are two source signals, x_1 and x_2 are the probe output signals, and k_{ij} are the transfer functions that represent the signal mixing (see Fig. 1).

Let us consider now a special case when the probe 2 is coupled to the source s_1 only, so $k_{22} = 0$ (in this case the probe 2 is the reference probe with respect to s_1). Then the ratio of the probe signals can be written as

$$\frac{x_1}{x_2} = \frac{k_{11}s_1 + k_{12}s_2}{k_{21}s_1} = \frac{k_{11}}{k_{21}} + \frac{k_{12}s_2}{k_{21}s_1}. \tag{8}$$

As demonstrated in [16], if 1) the probability distributions of variables s_1 and s_2 are symmetrical, 2) the signals are not correlated (i.e., s_1 and s_2 are independent random variables), and 3) $|s_1| > 0$ (these three conditions are true most signals as demonstrated in [16]), the mean value of the ratio (8) (given by the operator $\langle\cdot\rangle$) is equal to a constant

$$\left\langle \frac{x_1}{x_2} \right\rangle = \frac{k_{11}}{k_{21}} + \frac{k_{12}}{k_{21}}\frac{s_2}{s_1} = \left\langle \frac{k_{11}}{k_{21}} \right\rangle. \tag{9}$$

The amplitude of the contribution of the source s_1 to the probe signal x_1 by definition is equal to $|k_{11}s_1|$, and therefore the average power in the probe 1 due to the signal s_1 is

$$P_{11} = \langle |k_{11}s_1| \rangle^2. \tag{10}$$

At the same time, under the condition $k_{22} = 0$, s_1 can be related to x_2 as follows [using (7)]:

$$s_1 = \frac{x_2}{k_{21}}. \tag{11}$$

Substituting (11) to (10) the power contribution of s_1 can be obtained as

$$P_{11} = \left\langle \left| \frac{k_{11}x_2}{k_{21}} \right| \right\rangle^2. \tag{12}$$

According to (9), $\frac{k_{11}}{k_{21}} = \langle \frac{x_1}{x_2} \rangle$ and the power therefore is

$$P_{11} = \langle |x_2| \rangle^2 \left| \left\langle \frac{x_1}{x_2} \right\rangle \right|^2 \tag{13}$$

which means that the signal power contribution can be calculated by multiplying the averaged power in the reference channel $\langle |x_2| \rangle^2$ by the square of the absolute value of the mean of the ratio of the two probe signals.

If s_1 represents the intended signal, its power contribution to the probe 1 can be measured directly using (13). However, if s_1 represents noise, the contribution of the intended signal s_2 is of primary interest. It can be found by expressing $k_{12}s_2$ from (6) and using (11) and (9) as

$$\begin{aligned} k_{12}s_2 &= x_1 - k_{11}s_1 = x_1 - \frac{k_{11}}{k_{21}}x_2 \\ &= x_1 - x_2 \left\langle \frac{x_1}{x_2} \right\rangle. \end{aligned} \tag{14}$$

Then, the averaged power contribution of the signal s_2 to the probe 1 is

$$P_{12} = \left\langle \left| x_1 - x_2 \left\langle \frac{x_1}{x_2} \right\rangle \right|^2 \right\rangle. \tag{15}$$

If the reference signal is available [as in Fig. 1(a)], formulas (13) and (15) can be used directly to find the power contributions of both signals. However, if it is not, the signals need to be separated first by the BSS method as described in Section II-A, and then the separated signals can be used as references. It should be noted here that the result of (13) does not depend on k_{21} (the transfer coefficient in the reference channel), in other words, the procedure is immune to the arbitrary scaling of the signals during the BSS.

Assuming that the signals $\hat{s}_1$ and $\hat{s}_2$ represent the scaled references obtained by the BSS (i.e., the rows of the matrix $\hat{\mathbf{S}}$ in) and that they are correctly identified, i.e., the signal $\hat{s}_1$ is the reference to s_1 and $\hat{s}_2 - s_2$, the contributions of the signals measured by both probes, according to (13) are

$$P_{11} = \langle |\hat{s}_1| \rangle^2 \left| \left\langle \frac{x_1}{\hat{s}_1} \right\rangle \right|^2 \tag{16a}$$

$$P_{12} = \langle |\hat{s}_2| \rangle^2 \left| \left\langle \frac{x_1}{\hat{s}_2} \right\rangle \right|^2 \tag{16b}$$

$$P_{21} = \langle |\hat{s}_1| \rangle^2 \left| \left\langle \frac{x_2}{\hat{s}_1} \right\rangle \right|^2 \tag{16c}$$

$$P_{22} = \langle |\hat{s}_2| \rangle^2 \left| \left\langle \frac{x_2}{\hat{s}_2} \right\rangle \right|^2. \tag{16d}$$

Or, alternatively, by using (15)

$$P_{11} = \left\langle \left| x_1 - \hat{s}_2 \left\langle \frac{x_1}{\hat{s}_2} \right\rangle \right| \right\rangle^2 \tag{17a}$$

$$P_{12} = \left\langle \left| x_1 - \hat{s}_1 \left\langle \frac{x_1}{\hat{s}_1} \right\rangle \right| \right\rangle^2 \tag{17b}$$

$$P_{21} = \left\langle \left| x_2 - \hat{s}_2 \left\langle \frac{x_2}{\hat{s}_2} \right\rangle \right| \right\rangle^2 \tag{17c}$$

$$P_{22} = \left\langle \left| x_2 - \hat{s}_1 \left\langle \frac{x_2}{\hat{s}_1} \right\rangle \right| \right\rangle^2. \tag{17d}$$

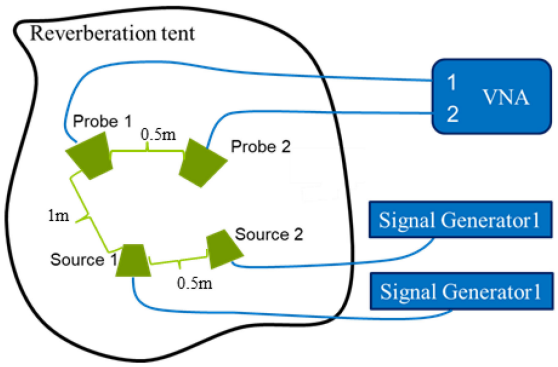

(a)

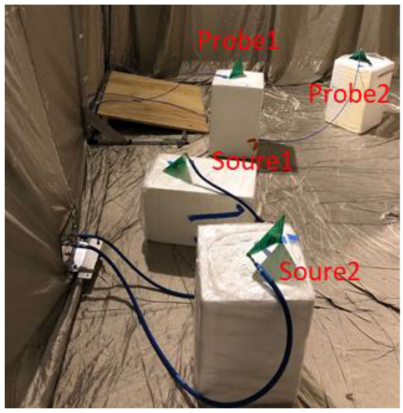

(b)

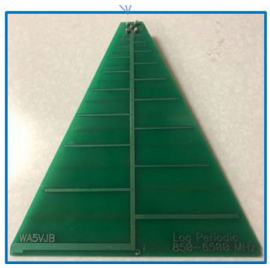

(c)

Fig. 2. (a) TRP measurement setup. The distance between the probes and the sources is around one meter. (b) The distance between the probes and between the sources is around 0.5 m. Actual configuration inside the tent. (c) Close-up photo of the log-periodic antenna.

III. Experimental Validation of the Method

A. Introduction of the Validation Test Setup

Fig. 2 shows the diagram of the measurement setup. The TRP measurement is performed in the reverberation tent, and the setup, in general, corresponds to (6) and (7), with k_{ij} being the transfer coefficients between transmitting and receiving antennas.

In this validation test, the intended signal and the noises are both sinusoidal signals, and both sensor probes are put inside the tent, implementing the case in Fig. 1(b) (no dedicated signal reference).

Signal generator 1 produces a 1-GHz sinusoidal signal with an amplitude of 5 dBm (Source 1). Signal generator 2 produces a 1.0005-GHz sinusoidal signal with an amplitude of 10 dBm (Source 2). The 500-kHz frequency difference was introduced to facilitate discrimination of the signals after the BSS procedure by observing their phase progressions. Since the signal generators are not referenced to each other, the signals produced by them are uncorrelated regardless of the nominal frequency difference. Four identical log-periodic antennas [Fig. 2(c)] working in the frequency range from 850 to 6500 MHz are used as emitting antennas and receiving probes. According to the datasheet [17], the reflection coefficient of the antenna does not exceed -8.45 dB in the working frequency range, and the antenna factor around 1 GHz is 24 dB(1/m).

The vector network analyzer is used as the measurement instrument. The center frequency is set to 1 GHz with zero span. The IF bandwidth is set to 1.5 MHz, such that both signals fall into the bandwidth, which makes them indistinguishable in the frequency domain (otherwise, the signal separation task could be done trivially just by tuning to the corresponding signal frequencies).

The power calculation procedure explained in Section II-B assumes that the coefficients k_{ij} are time-invariant. However, in the reverberation tent, the transfer coefficients between the antennas are constantly changing due to the movement of the tent's walls. On the other hand, that movement is relatively slow, with typical shaking "period" on the order of a second or a fraction of a second at worst. So, if averaging in (13) or (15) is performed within a short time (relative to the typical wall movement time), the transfer coefficients might be treated as quasi-static values. In the measurement, the sweep time of the VNA was set to 10 ms, which is presumably 10 to 100 times faster than the tent shaking quasi-period.

The signals in two channels must be recorded simultaneously to avoid losing correlations between probe signals x_1 and x_2. For this reason, the number of resolvable sources is practically limited to the number of channels of the measurement instrument.

Power received by the probe in each sweep is given by (13) (it is, of course, different for each sweep due to movement of the tent walls). The TRP, however, can be estimated by averaging the power (13) over the VNA sweeps (simultaneously with the tent stirring), similarly to a normal TRP measurement in the reverberation tent. If the references are obtained by the BSS, the TRP is obtained by averaging (16a) as

$$\mathrm{TRP}_{11} = \overline{P_{11}} = \overline{\langle|\hat{s}_1|\rangle^2 \left\langle \left| \frac{x_1}{\hat{s}_1} \right| \right\rangle^2} \tag{18}$$

and so on according to (16a)–(16d) or (17a)–(17d), where $\langle\cdot\rangle$ represents averaging over all samples within one sweep and $\overline{\cdot}$ represents averaging over the sweeps.

For validation purposes, the contribution of each source is also measured directly with only one of the signal generators turned ON.

B. Measurement Results

Fig. 3 shows the contributions of the sources obtained by measuring the signals with only one of the sources turned ON

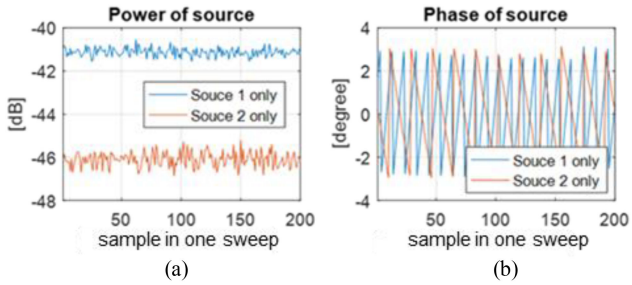

Fig. 3. (a) Power and (b) phase of the individual sources (one sweep).

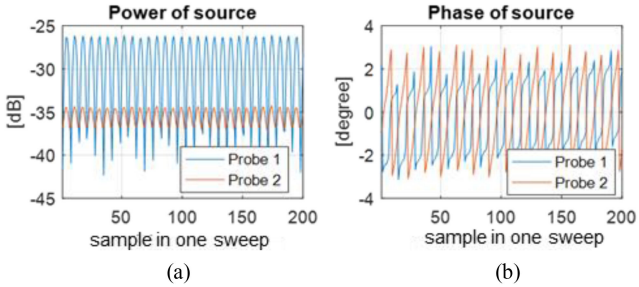

Fig. 4. (a) Power and (b) phase of the mixed signals (one sweep).

(measured by one of the probes). The measurements are performed within one 10-ms sweep. As can be seen, the amplitudes are practically time-independent (besides small variations due to the additive instrument noise), which demonstrates that the tent can be treated as a time-invariant system within the sweep time (10 ms). The slope of the phases allows to identify signals, i.e., source 1 (1-GHz carrier) has a decreasing phase progression, and source 2 (1.0005-GHz carrier) has an increasing phase progression. In a more practical case of active electronic devices, signal identification would require detecting signatures in the signals (phase progression, data pattern, etc.), which have to be analyzed prior to the TRP measurement (see examples in Section IV).

Fig. 4 shows the measurement result of the mixed signals (i.e., when both generators are turned ON). Compared to the signals due to the individual sources, the amplitude in the probe channels becomes time-dependent (due to beats of two sinusoidal signals with different frequencies). The phase progression loses its linearity.

Fig. 5 shows the mean powers in both probe channels measured over 300 sweeps. The power is different for each sweep, which is caused by the stirring of the chamber. The average values over the sweeps converge when the chamber is thoroughly stirred [18]. The mean power of contributions measured directly (by disabling the other source) for Source 1 is -39.6 dBm, and for the Source 2 is -32.1 dBm (without compensation of the antenna and cable factors and the tent loss).

To resolve the individual contribution of the emission sources, the BSS is applied to the mixed probe signals to obtain the references. An example of the separated signals obtained in one sweep is shown in Fig. 6. As can be seen, it reproduces

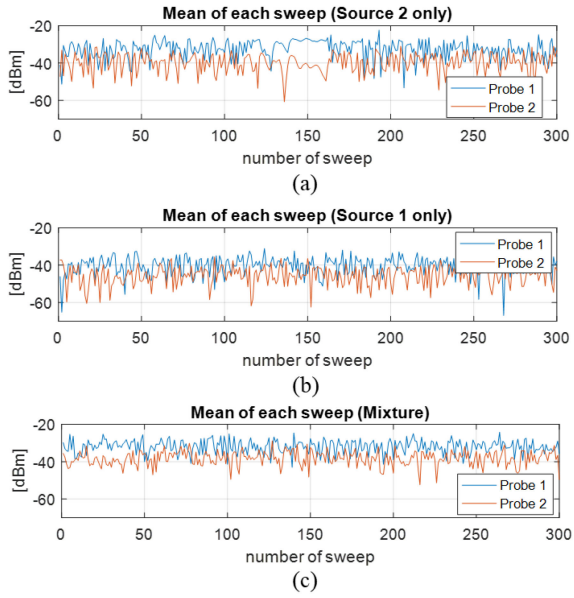

Fig. 5. Output amplitude in measurement probes for (a) Source 1, (b) Source 2, and (c) mixed case (mean values within each sweep).

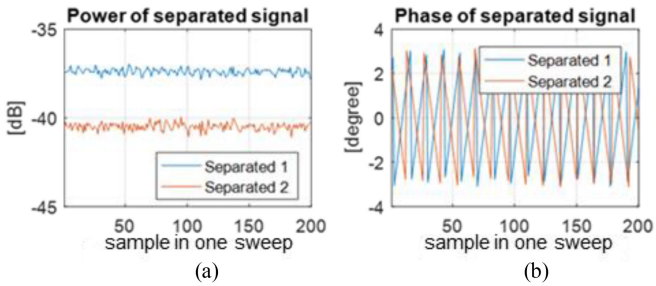

Fig. 6. (a) Amplitude and (b) phase of the separated signals in one sweep.

TABLE I
AMPLITUDE OF THE TRP CONTRIBUTIONS MEASURED DIRECTLY AND RESOLVED FROM THE MIXTURE USING BSS

	Source 1	Source 2
Direct Measurement	-39.6dBm	-32.1dBm
Separated	-40.0dBm	-34.9dBm

the signals in Fig. 3 almost perfectly (with respect to unknown scaling), demonstrating successful separation.

The order of the separated results is arbitrary, and the signals are identified by their phase progression.

After obtaining the separated results in each sweep using (3) and (4), the average cancelation method according to (16) is used to calculate the power contributions to the probe 1, and finally, the TRPs are obtained by averaging over multiple sweeps (18). The results of this procedure are listed in Table I (labeled "separated") and compared to the direct TRP measurements.

As can be seen, the separated results are in good agreement with the ones measured directly. The largest difference (2.8 dB) is observed for the source 2, which is comparable to a typical measurement uncertainty in a reverberation chamber [19], [20].

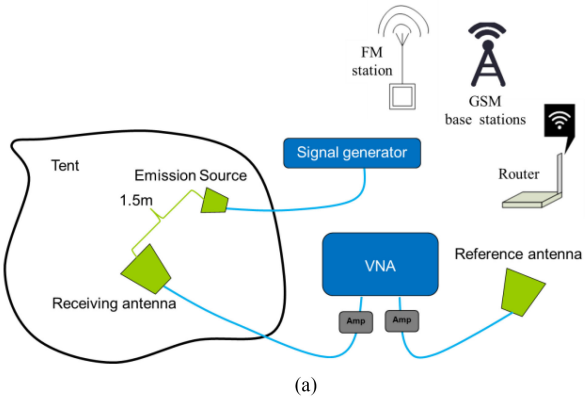

(a)

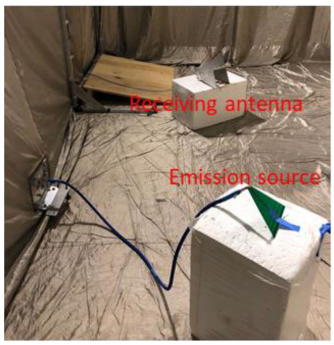

(b)

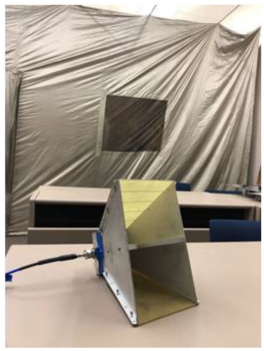

(c)

Fig. 7. (a) Measurement setup with dedicated noise reference. (b) Real configuration inside the tent. (c) Outside the tent.

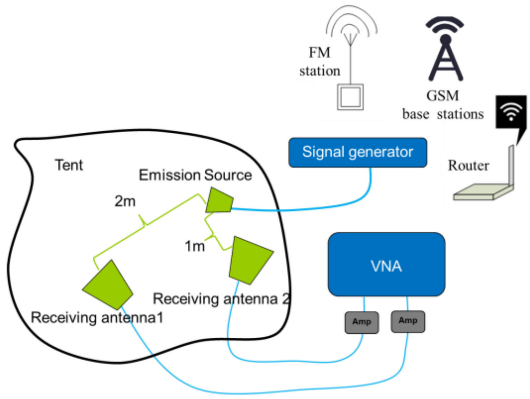

(a)

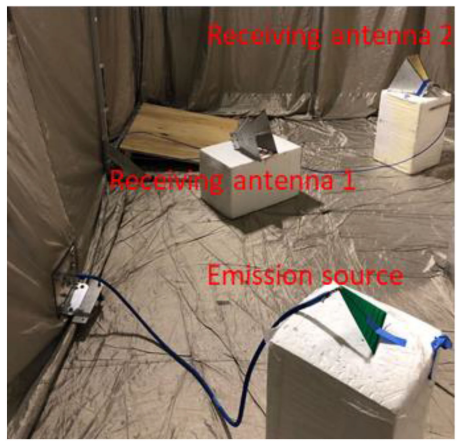

(b)

Fig. 8. (a) Measurement setup with no dedicated noise reference. (b) Real configuration inside the tent.

IV. Active Noise Application

Wi-Fi, FM, and GSM are three common communication signals that are widespread in daily life and in testing environments. In EMI measurements it is essential to eliminate the effects of interference of such signals. This is usually achieved by shielding. However, sometimes, the shielding is insufficient (especially in reverberation tents).

In this section, the TRP measurement is implemented in the reverberation tent. The signal generator modeling the intended signal source produces sinusoidal signals at the same frequency as the communication noises. The vector network analyzer is used as the measurement instrument. The noises existing in the testing environment are generated by external (relative to the tent) sources such as the Wi-Fi routers, FM stations, and GSM base station/cellphones. The measurements are performed at a fixed frequency with zero span. In the measurement, the sweep time of the VNA was set to 10 ms to ensure the quasi-static nature of the tent measurements. The signals in two channels are recorded simultaneously to avoid losing correlations between measured signals.

Fig. 7 shows the setup with the dedicated noise reference [corresponding to Fig. 1(a)]. The reference antenna is placed outside the tent at a considerable distance such that the coupling to it from the intended sources is negligible.

Fig. 8 shows the setup with no dedicated reference [corresponding to Fig. 1(b)]. In this case, both antennas are placed inside the tent and are coupled to both sources.

In both setups, a log-periodic antenna [16] is used as an emission source, and double-ridged horns [20] are used as receiving probes.

A. Wi-Fi Signal Cancelation

Wi-Fi is a family of radio technologies commonly used for wireless local area networking (WLAN) of devices, based on the IEEE 802.11 family of standards. The 802.11 standard provides several distinct radio frequency ranges for use in Wi-Fi communications: 900 MHz; 2.4, 3.6, 4.9, 5, 5.9, and 60 GHz bands. Each range is divided into a number of channels. Fourteen channels are designated in the 2.4-GHz range, spaced 5-MHz apart from each other except for a 12-MHz space before channel 14.

For the presented study, a frequency of 2.46 GHz is selected as the frequency of interest, and the measurements are performed according to Fig. 7. Fig. 9 shows the Wi-Fi signal in the reference (red curve) and the signal (blue curve) channels measured at 2.46 GHz within one zero-span sweep. The Wi-Fi signal occurs intermittently, and between the peaks, the recorded signal in the reference channel is the instrument noise. As such, the measurement cannot be described by the model presented above in (6) and (7) (the instrument noise is not negligible and cannot be avoided. Therefore the model should include at least three

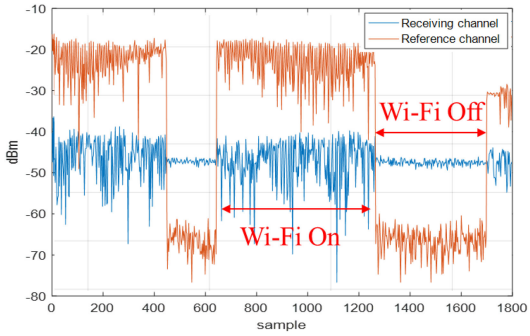

Fig. 9. Magnitude measured by the two antennas in one sweep.

signals). Because of this, the ratio averaging (9) cannot be used to cancel the Wi-Fi signal. However, it is possible to use the intermittent nature of the signal to perform cancelation.

In the periods when the Wi-Fi signal is OFF, the signal from the signal generator is received in the tent without any interference. When the Wi-Fi is ON, the signal channel receives both the emission and the noise, and the waveform becomes noisy. By defining a threshold V_T in the reference channel between the levels of the Wi-Fi signal peaks and the instrument noise it is possible to define the measured signal as

$$V_{\text{meas}} = \begin{cases} V_{sig}, & V_{ref} < V_T \\ \emptyset, & V_{ref} \geq V_T \end{cases} \tag{19}$$

where V_{sig} is the signal measured at the output of the antenna placed in the tent, V_{ref} is the noise reference signal (output of the reference probe outside the tent), and the symbol $\emptyset$ indicates that no values are assigned to the measured signal. The threshold treatment (19) ensures that the intentional signal is measured only when the source of the Wi-Fi signal is not active. Of course, this strategy would work only if the intentional signal is not strongly correlated to the Wi-Fi signal (otherwise it will be cancelled as well).

The power of the intentional signal is then calculated as

$$\text{TRP}_{\text{meas}} = \overline{\langle |V_{\text{meas}}| \rangle^2}. \tag{20}$$

When no direct reference is available (as in the setup described in Fig. 8.), it is much harder to detect the moments when the Wi-Fi signal is OFF (due to the decreased signal-to-noise ratio). In this case, the BSS can be applied to the signals measured by two receiving antennas to increase the SNR. And while the BSS cannot separate the signals perfectly (because of the nonnegligible contribution due to the instrument noise), it can increase the SNR in the reference channel and facilitate the threshold processing procedure (19). Fig. 10 shows the measured and separated result over one sweep. As can be seen, the partially separated Wi-Fi signal (red curve) has a much larger dynamic range compared to the mixed case, which makes it more suitable for the reference in (19).

In the results presented below, the power is averaged over 300 sweeps. Each sweep contains 1800 sample points before the threshold elimination (19).

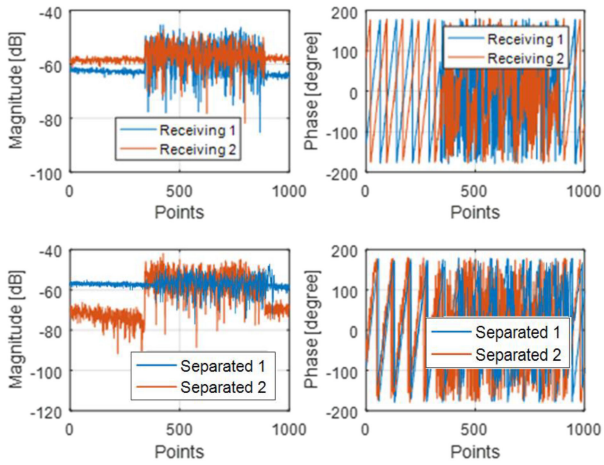

Fig. 10. Measured and resolved result with indirect reference over one sweep.

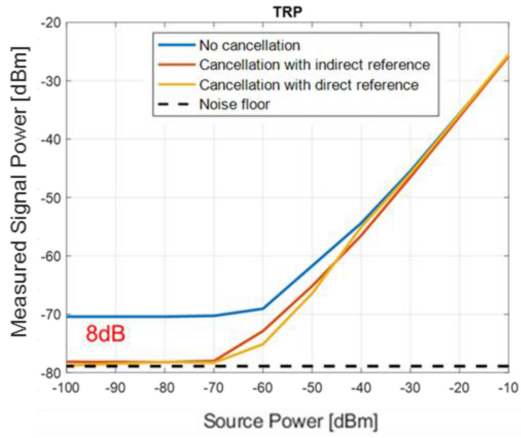

Fig. 11. Result of the Wi-Fi noise cancelation.

Fig. 11 shows a comparison between the measured signal power with and without the Wi-Fi noise cancelation as a function of the signal generator output power. When the signal is strong enough, the influence of the Wi-Fi noise is negligible, and the curve is linear. However, as the signal power decreases, eventually, the measured power converges to the Wi-Fi contribution (the blue curve thresholds at -70 dBm), which is approximately 10-dB above the instrument noise floor. However, the threshold treatment with both direct and indirect (obtained by BSS) noise references allows to measure the signal power accurately down to the instrument noise floor, increasing the dynamic range of the measurement by approximately 8 dB.

B. GSM Signal Cancelation

The Global System for Mobile Communications (GSM) is a standard developed by the European Telecommunications Standards Institute (ETSI) to describe the protocols for second-generation (2G) digital cellular networks used by mobile devices such as mobile phones and tablets.

The GSM signal spectrum measured in the test environment within the 1900-MHz band is shown in Fig. 12. As can be seen,

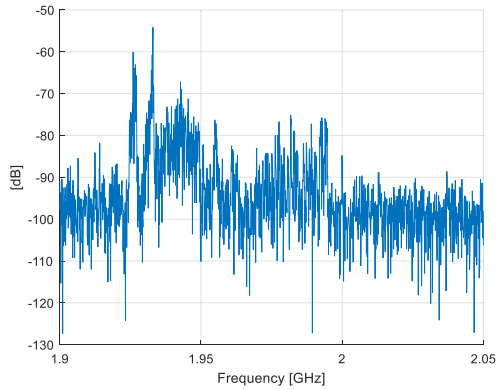

Fig. 12. Spectrum of the GSM signal measured in the test environment.

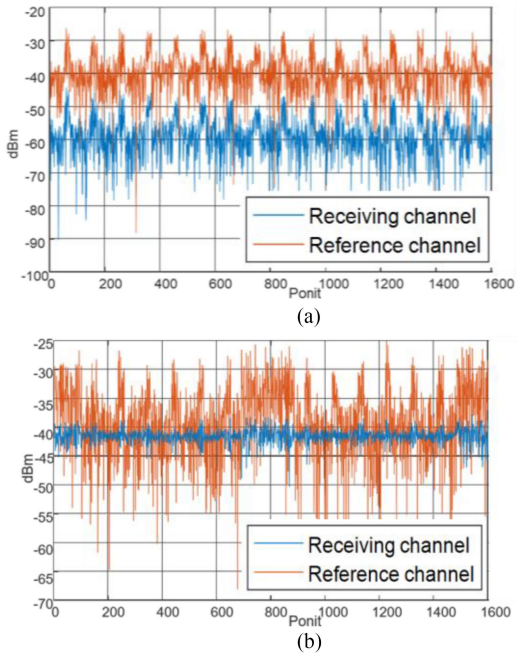

Fig. 13. Examples of mixed signals measured at 1.932 GHz over one sweep. (a) Emission source is OFF. (b) Emission source is ON.

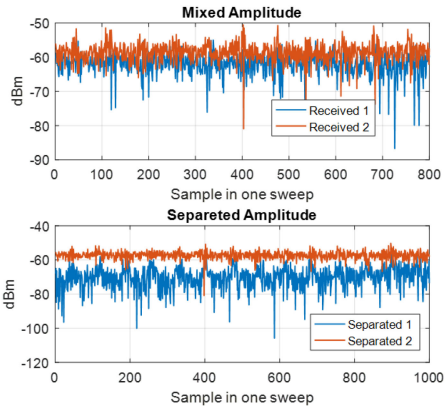

Fig. 14. Magnitude in two channels in one sweep before and after separation.

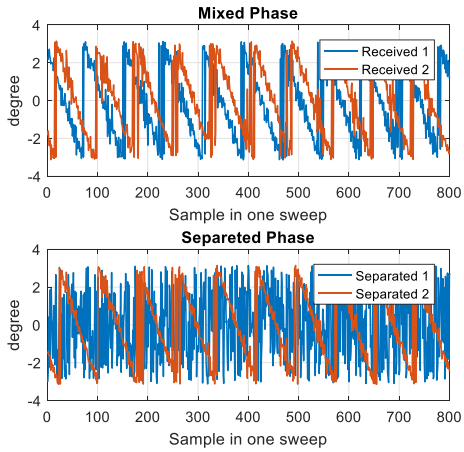

Fig. 15. Phase in two channels in one sweep before and after separation.

the noise signal has a peak at 1.932 GHz, and the intended signal generator was tuned to this frequency to represent the worst case (in terms of the SNR).

In contrast to the Wi-Fi signal, the GSM signal is continuous (albeit time-variant), as is shown in Fig. 13 (measurements are done according to Fig. 7). Fig. 13(a) represents the signals measured with the signal generator OFF. As can be seen, both channels capture the GSM signal. When the generator is ON [Fig. 13(b)], the antenna inside the tent captures a mixture of the GSM and sinusoidal signal, while the external reference antenna receives the GSM signal only.

For the scenario with a direct noise reference signal (Fig. 7), the intended signal contribution can be calculated using (15). For the scenario without the direct reference (Fig. 8), BSS is needed to obtain the reference.

Figs. 14 and 15 show a comparison between the measured signals obtained in the setup with no dedicated reference (Fig. 8) and the BSS-resolved results. By comparing the phase before and after separation, it can be seen that the intended signal (linear phase progression) is successfully separated from the GSM noise (random phase).

After obtaining separated signals in each sweep, the average cancelation method is used to calculate the powers of the two signals, and finally, the TRP is obtained by averaging over multiple sweeps (18). The results of this procedure are plotted in Fig. 16.

Both cancelation methods (with direct and indirect reference) were, however, able to improve the dynamic range by 7.5 dB without reaching the noise floor. A possible reason for that is that the received GSM signals originate from multiple base stations and cell phones. As a result, the signals measured in different locations are not perfectly correlated, which violates the mixing model (6) and (7). To investigate the reason for poor suppression of the GSM signal, the coherence coefficient between signals picked up by two antennas was measured in the setup shown in Fig. 17.

The coherence coefficient (sometimes called magnitude-squared coherence) between two signals $x(t)$ and $y(t)$ is a

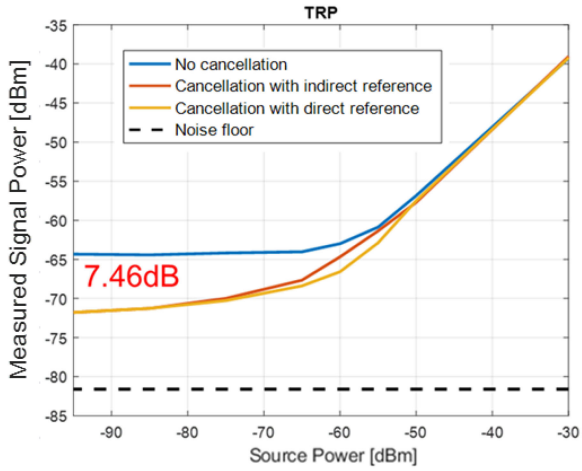

Fig. 16. Result of the GSM noise cancelation at 1.932 GHz.

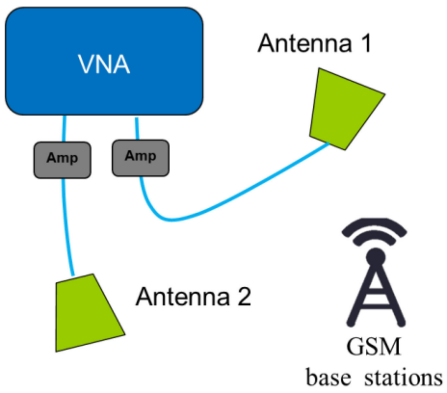

Fig. 17. Setup for the GSM signal coherence measurement.

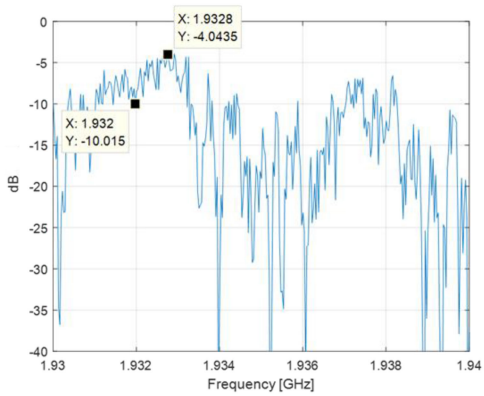

Fig. 18. Coherence between two signals measured in the setup in Fig. 17.

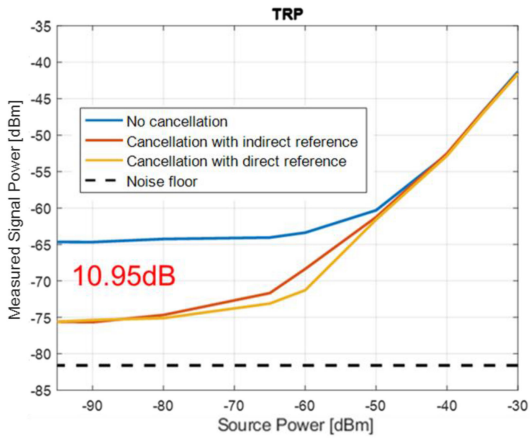

Fig. 19. Result of the GSM noise cancelation at 1.9328 GHz.

real-valued function that is defined as

$$\gamma = \frac{|S_{xy}(f)|^2}{S_{xx}(f)\,S_{yy}(f)} \tag{21}$$

where $S_{xy}(f)$is the cross-spectral density between x and y, $S_{xx}(f)$,and $S_{yy}(f)$ are the autospectral density of x and y, respectively. The coefficient is equal to 1 for perfectly correlated signals, and to 0 for uncorrelated signals.

The measurements in Fig. 17 are performed outside the tent due to the difficulty of measuring the power terms in (21) in a geometrically unstable tent. And while the spatial coherence of the electromagnetic field inside and outside the tent, in general, can be different, we assumed that the frequency behavior of the coherence coefficient is similar, i.e., larger values will be observed at the same frequencies inside and outside the tent.

The results of the coherence coefficient measured between the GSM signals picked up by two antennas placed at 2.5-m distance in the frequency range from 1.93 to 1.94 GHz are presented in Fig. 18 (a VNA in the tuned receiver mode was used to measure the signals). As can be seen, the coherence coefficient at the selected frequency of 1.932 is relatively low (-10 dB). To demonstrate that the suppression level depends on the coherence, the cancelation procedures described above were repeated at 1.9328 GHz, where the coherence is significantly higher (-4 dB), however, it is still not perfect. Corresponding results are shown in Fig. 19. Compared to Fig. 18, the GSM signal suppression is improved by roughly 3 dB, reaching 11 dB. However, the noise floor was not reached still, which agrees with the expectation regarding suppression of partially correlated signals.

C. FM Cancelation

FM broadcasting is used worldwide to provide high-fidelity sound over broadcast radio. The FM spectrum measured in the test environment is shown in Fig. 20. In this case, the cancelation is performed for the signal of the station broadcasting at 99.7 MHz. Custom wire antennas were used to measure the signals.

Similar to the GSM signal, the FM signal is also a continuous time-variant signal and can be processed in the same way as the GSM signal. For the scenario with direct reference (Fig. 7), the power contribution can be calculated using (15). For the scenario in Fig. 8, BSS is used to obtain the reference.

Figs. 21 and 22 show a comparison between the directly measured signals and the separated results in the indirect reference setup. By observing magnitude and phase after separation,

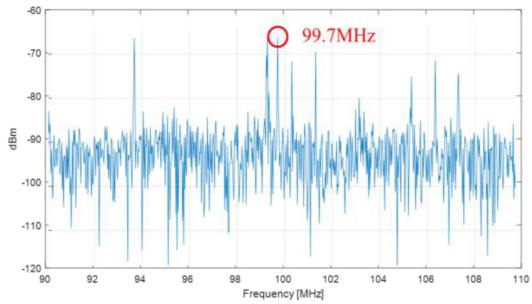

Fig. 20. Spectrum of FM measured in the test environment.

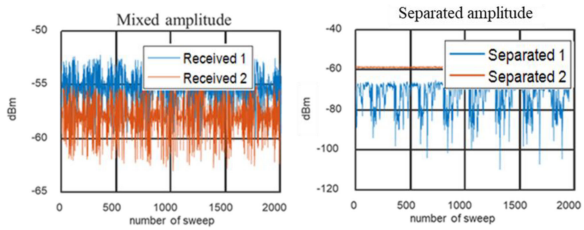

Fig. 21. Mixed and separated amplitudes with FM noise measured in one sweep

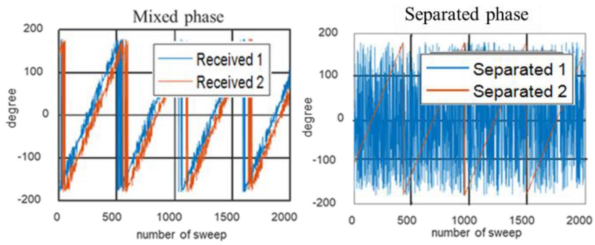

Fig. 22. Mixed and separated phases with FM noise measured in one sweep.

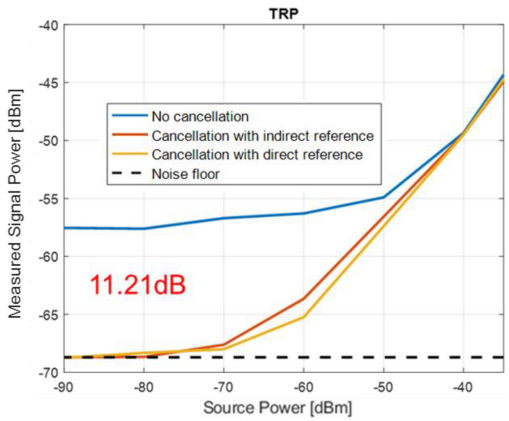

Fig. 23. Result of the FM noise cancelation at 99.7 MHz.

it is easy to identify the intended signal (red curve–constant amplitude, linear phase) and the FM interference signal (blue curve–time-varying amplitude, noise-like phase).

The results of the TRP measurements for direct and indirect references are plotted in Fig. 23.

Both the direct and indirect reference methods suppress the FM noise efficiently, extending the dynamic range of the measurement down to the noise floor (11-dB increase).

V. Conclusion

Practical methods are proposed for suppression of unintentional noise signals of different nature for the TRP measured in the reverberation tent, allowing in many cases to extend the dynamic range of the measurement down to the noise floor of the receiving instrument. The TRP contributions can be related to the sources by examining signal signatures (such as phase progression, data pattern, etc.). Practical aspects of signal identifications in complex electronic systems deserve additional investigation.

In the case of intermittent interference signals like Wi-Fi, setting a threshold for the noise reference (measured directly or obtained by the BSS) allows to exclude the portions of the signal corrupted by the Wi-Fi noise.

In the case of continuous signals like GSM and FM, ratio averaging allows canceling the uncorrelated part. The power contribution of the intended signal can be achieved after the cancelation. When the interference reference signal is not available, the blind source separation method allows the references to be obtained from the mixture. In order to avoid the influence of the tent stirring the BSS is implemented within relatively short time periods (10 ms).

Similar methods can be applied to other scenarios when the unwanted interference signal needs to be suppressed, for example during field scan or open area test site (OATS) measurements.

References

[1] J. Meiguni *et al.*, "System level EMC for multiple EMI sources," in *Proc. IEEE Int. Symp. Electromagn. Compat., Signal Power Integrity*, New Orleans, LA, USA, 2019, pp. 493–498.

[2] Y. Zhong *et al.*, "Measurement-based quantification of buzz noise in wireless devices," in *Proc. Joint Int. Symp. Electromagn. Compat., Sapporo Asia-Pacific Int. Symp. Electromagn. Compat.*, Sapporo, Japan, 2019, pp. 552–555.

[3] J. Xu, F. Dai, D. Su, Q. Qiao, and H. Zheng, "Ambient noise cancellation in frequency domain EMI measurement," in *Proc. 4th IEEE Int. Symp. Microw. , Antenna, Propag. EMC Technologies for Wireless Commun.*, 2011, pp. 555–558.

[4] J. C. West and C. F. Buntling, "An analysis of reverberation chamber testing as a radiation problem," in *Proc. IEEE Symp. Electromagn. Compat. , Signal Integrity Power Integrity*, Long Beach, CA, USA, 2018, pp. 616–621.

[5] C. L. Holloway *et al.*, "On the use of reverberation chambers to simulate a Rician radio environment for the testing of wireless devices," *IEEE Trans. Antennas Propag.*, vol. 54, no. 11, pp. 3167–3177, Nov. 2006.

[6] F. Leferink, J. -C. Boudenot, and W. van Etten, "Experimental results obtained in the vibrating intrinsic reverberation chamber," in *Proc. IEEE Int. Symp. Electromagn. Compat.*, Washington, DC, USA, 2000, pp. 639–644, vol. 2.

[7] W. S. Gan, S. Mitra, and S. M. Kuo, "Adaptive feedback active noise control headset: Implementation, evaluation and its extensions," *IEEE Trans. Consum. Electron.*, vol. 51, no. 3, 975–982, Aug. 2005.

[8] S. M. Kuo, S. Mitra, and W.-S. Gan. "Active noise control system for headphone applications," *IEEE Trans. Control Syst. Technol.*, vol. 14, no. 2, pp. 331–335, Mar. 2006.

[9] C. Osterwise, S. L. Grant, and D. Beetner, "Reduction of noise in near-field measurements," in *Proc. IEEE Int. Symp. Electromagn. Compat.*, Fort Lauderdale, FL, USA, 2010, pp. 171–176.

[10] A. Frech, S. Braun, and P. Russer, "Time-domain EMI measurements in the presence of ambient noise," in *Proc. 2009 IEEE Int. Symp. Electromagn. Compat.*, Austin, TX, USA, 2009, pp. 139–142.

[11] T. Li, V. Khilkevich, and D. Pommerenke, "Phase-resolved near-field scan over random fields," *IEEE Trans. Electromagn. Compat.*, vol. 58, no. 2, pp. 506–511, Apr. 2016.
[12] W. L. Zhou and D. Chelidze, "Blind source separation-based vibration mode identification," *Mech. Syst. Signal Process.*, vol. 21, no. 8, pp. 3072–3087, Nov. 2007.
[13] L. Parra and P. Sajda, "Blind source separation via generalized eigenvalue decomposition," *J. Mach. Learn. Res.*, vol. 4, no. 7-8, pp. 1261–1269, Oct./Nov.15, 2004.
[14] Y. Liu, R. He, J. Li, and V. Khilkevich, "Measurement of the total radiated power contributions in a reverberation tent," in *Proc. IEEE Int. Symp. Electromagn. Compat., Signal Power Integrity*, New Orleans, LA, USA, 2019, pp. 654–657.
[15] Comon, P. and C. Jutten, *Handbook of Blind Source Separation: Independent Component Analysis and Applications*. New York, NY, USA: Academic Press, 2010.
[16] A. Patnaik *et al.*, "Source isolation measurements in a multi-source coupled system," in *Proc. IEEE Int. Symp. Electromagn. Compat. Signal/Power Integrity*, Washington, DC, USA, 2017, pp. 75–80.
[17] Kent Electronics, "Datasheet of log periodic printed circuit board antennas: 850–6500 MHz," Accessed: Apr. 2020, [Online]. Available: https://www.wa5vjb.com/pcb-pdfs/LP8565.pdf
[18] Q. Xu and Y. Huang, "Measurement uncertainty in the reverberation chamber," in *Anechoic Reverberation Chambers: Theory, Design, and Measurement*, Hoboken, NJ, USA: Wiley, 2018, pp. 283–303.
[19] C. L. Holloway, P. F. Wilson, G. Koepke, and M. Candidi, "Total radiated power limits for emission measurements in a reverberation chamber," in *Proc. IEEE Symp. Electromagn. Compat. Symp. Rec.*, Boston, MA, USA, 2003, vol. 2, pp. 838–843.
[20] S. J. Boyes, Y. Huang, and N. Khiabani, "Assessment of UWB antenna efficiency repeatability using reverberation chambers," in *Proc. IEEE Int. Conf. Ultra-Wideband*, Nanjing, China, 2010, pp. 1–4, doi: 10.1109/ICUWB.2010.5615264.
[21] "Datasheet of 3115 Double-ridged Guide Antenna," ETS-Lindgren, Cedar Park, TX, USA, Accessed April, 2020: http://www.ets-lindgren.com/datasheet/antennas/ double-ridged-guide/4002/400203

Yuanzhuo Liu (Student Member, IEEE) received the B.E. degree in electrical and computer engineering from the Huazhong University of Science and Technology, Wuhan, China, in 2017, and the M.S. degree in electrical engineering from Missouri University of Science and Technology (formlerly University of Missouri–Rolla), Rolla, MO, USA, in 2019, where she is currently working toward the Ph.D. degree in electrical engineering with EMC Laboratory, Missouri University of Science and Technology.

Her research interests include electromagnetic interference, signal integrity in high-speed digital systems, and microwave imaging.

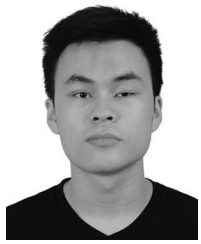

Sheng Guo received the B.S. degree in electromagnetic field and wireless communication from Huazhong University of Science and Technology, Wuhan, China, in June 2020.

He worked as Intern with EMC Laboratory of Missouri University of Science and Technology, Rolla, MO, USA, from June to October 2019. His research interests include electromagnetic interference, electromagnetic compatibility, microwave techniques, and RFIC.

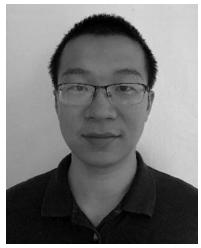

Ruijie He (Student Member, IEEE) was born in Hubei, China, in 1994. He received the B.S. in electrical engineering from Huazhong University of Science and Technology (HUST), Wuhan, China, in 2015. He is currently working toward the Ph.D. degree with the EMC Lab, Missouri University of Science and Technology, Missouri University of Science and Technology, Rolla, MO, USA.

He has been a Graduate Research Assistant, since 2015. His topics of interests are EMI modeling, HF modeling of power circuits, and electromagnetic compatibility.

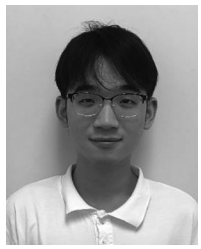

Jiangshuai Li (Student Member, IEEE) received the B.E. degree in electrical and computer engineering from the Huazhong University of Science and Technology, Wuhan, China, in 2017. He is currently working toward the M.S. degree in electrical engineering with the EMC Laboratory, Missouri University of Science and Technology (formerly University of Missouri Rolla), Rolla, MO, USA.

His research interests include signal integrity in high-speed digital systems, microwave imaging, electromagnetic interference, and automotive electromagnetic modeling.

Victor Khilkevich (Member, IEEE) received the Ph.D. degree in electrical engineering from Moscow Power Engineering Institute, Technical University, Moscow, Russia, in 2001.

He is currently an Associate Research Professor with the Missouri University of Science and Technology, Rolla, MO, USA. His research interests include microwave imaging, automotive electromagnetic compatibility modeling, and high-frequency measurement techniques.